Wavenumber Analysis of Azimuthally Distributed Data: Assessing Maximum Allowable Gap Size

SYLVIE LORSOLO AND ALTUĞ AKSOY

Cooperative Institute for Marine and Atmospheric Studies, University of Miami, and Hurricane Research Division, NOAA/AOML, Miami, Florida

(Manuscript received 10 August 2011, in final form 20 January 2012)

ABSTRACT

Performing wavenumber decomposition on azimuthally distributed data such as those in tropical cyclones can be challenging when data gaps exist in the signal. In the literature, ad hoc approaches are found to determine maximum gap size beyond which not to perform Fourier decomposition. The goal of the present study is to provide a more objective and systematic method to choose the maximum gap size allowed to perform a Fourier analysis on observational data. A Monte Carlo–type experiment is conducted where signals of various wavenumber configurations are generated with gaps of varying size, then a simple interpolation scheme is applied and Fourier decomposition is performed. The wavenumber decomposition is evaluated in a way that requires retrieval of at least 80% of the original amplitude with less than 20° phase shift. Maximum allowable gap size is then retrieved for wavenumbers 0–2. When prior assessment of signal configuration is available, the authors believe that the present study can provide valuable guidance for gap size beyond which Fourier decomposition is not advisable.

1. Introduction

Understanding atmospheric phenomena such as tropical cyclones (TCs) usually involves in-depth study of their kinematic and thermodynamic structures. Although common practice often involves axisymmetric analyses of various fields, it is well known that TC internal processes are also modulated by asymmetric processes (e.g., Montgomery and Kallenbach 1997; Schubert et al. 1999). To investigate such asymmetries, azimuthal wavenumber decomposition of storm-relative fields is typically carried out. Vertical wind shear, for example, can cause low wavenumber asymmetric structures as seen in Reasor et al. (2000), whereas mesovortices can be identified in high wavenumber asymmetries (Aberson et al. 2006; Montgomery et al. 2006). The need to better understand both axisymmetric and asymmetric structure through observational data has further increased with the need to validate high-resolution model output.

Doppler radar data have increasingly become the primary source of observations to study hurricane structure (Marks et al. 1992; Roux and Marks 1996; Lee et al. 2000) and validate models (Nolan et al. 2009). However, retrieving wavenumber components of the kinematic fields has proven to be quite challenging, mainly because of missing data inherent in observational datasets (Reasor et al. 2009; Lee et al. 2000). Indeed, Doppler radar data often exhibit gaps azimuthally, which affects the quality of Fourier decompositions. Conversely, model kinematic fields are fully available on regular grids. To circumvent the problem, interpolation schemes are usually used to fill in the data gaps. A maximum allowable gap size is usually chosen beyond which a wavenumber decomposition is deemed not worth performing. Lee et al. (2000) restricted the missing data gap size as a function of the considered wavenumber (see Table 2 in their paper). However, reasons for the choice of the maximum gap size were not discussed in detail and were only valid for the tangential wind retrieved using the ground-based velocity track display (GBVTD) technique.

Recently, various studies investigating hurricane structure have used airborne Doppler analyses obtained from a variational method (Gamache 1997; Gao et al. 1999). These analyses provide three-dimensional wind

Corresponding author address: Sylvie Lorsolo, CIMAS, University of Miami, and NOAA/AOML/HRD, 4301 Rickenbacker Cswy., Miami, FL 33149-1097.
E-mail: sylvie.lorsolo@noaa.gov

DOI: 10.1175/MWR-D-11-00219.1

components and, if the quality of the wind retrieval permits, wavenumbers of kinematic fields can be computed (Reasor et al. 2009). However, storm structure and data quality can often cause a wide range of missing data at various radii from the storm center. Reasor et al. (2009) only performed Fourier decompositions for analyses where at least 60% of data were present. This threshold value was chosen after multiple tests, but was essentially a subjective choice (P. D. Reasor 2010, personal communication).

The intent of the present study is to provide a more objective and systematic method to choose the maximum data gap size allowed to perform a Fourier analysis on observational data. Although this study originally targets the problem of "gappy" data[1] in Doppler radar analyses of TCs, the issue of missing data is also encountered when studying other phenomena such as tornados, or other types of smaller-scale vortices embedded in a mean wind field. Thus, we foresee that the method presented here can be applied to a greater variety of azimuthally spaced observational datasets. A Monte Carlo experiment is designed to assess the quality of Fourier decompositions when taking into account signal shape, the position of the gap(s) in the signal, and the number and size of the gap(s).

2. Methodology

The goal of this paper is to implement a method that will provide a systematic way of choosing the largest gap allowed to compute the wavenumber components of an azimuthally varied signal. The method will help determine the maximum allowable gap size for Fourier decomposition depending not only on the signal shape, but also on the desired quality of the retrieved wavenumbers.

Because this study was initiated by the need to better understand the kinematic structure of TCs, the signal shapes discussed here will present similar characteristics to those of TCs. As an example, Fig. 1 presents sample tangential, radial, and vertical wind fields from a realistic model simulation of Hurricane Paloma (2008) and their associated amplitude spectra at 50 km from the storm center. The amplitude of wavenumber 0 (Fig. 1b) is much larger than that of the higher wavenumbers for the tangential wind while for the radial wind, wavenumber 1 largely dominates (Fig. 1d). The vertical wind presents a more complex picture (Fig. 1e), with higher wavenumbers explaining a large portion of the variance.

[1] In this study we will use the term "gappy" to mean missing data for brevity.

In this study a "dominant" wavenumber component is defined as one that accounts for about 50% of the total variance in the signal. The goal is to be able to determine the largest gap size that will permit the retrieval of various wavenumber components with a preset accuracy. For this study, only wavenumber 0, 1, and 2 (referred as $n = 0, 1,$ and 2, respectively) are retrieved. First, signals with specific wavenumber configurations are randomly generated, and then gaps are inserted at random places. These gaps are then filled with a chosen interpolation scheme and a Fourier decomposition is performed on the interpolated signal. The wavenumber components computed as such are then compared to the wavenumbers of the original signal with no gaps. The experiment is repeated multiple times to obtain statistically representative results.

a. Signal generation

The first step of the experiment is to generate signals from which the wavenumber components are computed. The signals are generated as linear combinations of various wavenumbers, and white noise is added as a proxy for energy at higher wavenumbers as described in Eq. (1):

$$X = A_0 + \left(\sum_{n=1}^{3} A_n \sin[n\theta + \phi_n] \right) + \xi, \qquad (1)$$

where θ is azimuth angle by which the signal is assumed to vary (at 1° resolution), A_n represents the amplitude of the wavenumber n component, Φ_n is phase, ξ represents white noise, and A_0 represents the mean value of the signal. The amplitude and white noise are randomly generated assuming normal distributions. The phase is random with an assumed uniform distribution within $[0, 2\pi]$. The standard deviation of the assumed normal distribution for amplitude is approximately 10% of the amplitude of the most energetic wavenumber.

Five types of signal are generated with specific wavenumber configurations described in Table 1. Individual wavenumber components are generated based on assumed variance explained and the following standard relationship between wave amplitude and variance:

$$\mathrm{Var}_n = \frac{A_n^2}{2}, \qquad (2)$$

where Var_n is the variance of the wavenumber n component and $n = 1, \ldots, 3$. For each configuration, A_0 is equal to the amplitude of the most energetic wavenumber(s) of each considered signal.

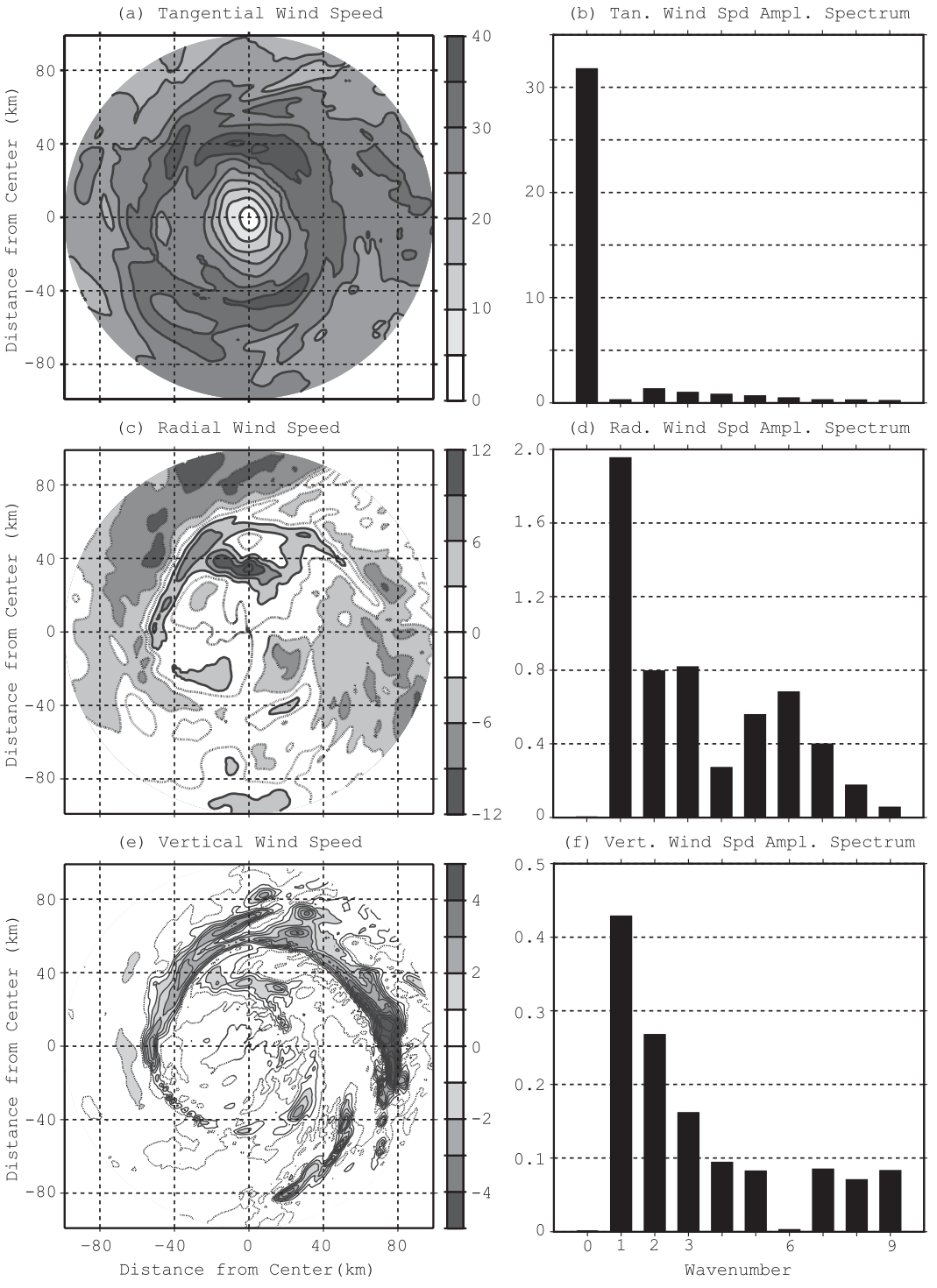

FIG. 1. Horizontal cross sections of (a) tangential, (c) radial, and (e) vertical wind speed (m s^{-1}) at 3-km height from the Hurricane Paloma (2008) nature run. Solid lines and dashed lines delineate positive and negative values, respectively. (b),(d),(f) The associated amplitude spectra (m s^{-1}) at 50 km from the storm center.

TABLE 1. Description of types of signal generated and assumed variance explained (%) by wavenumbers 1–3 when the percentage of additive noise is 10% [var(ξ) = 10% total variance].

Configuration	Dominant wavenumber	Percent variance explained when ξ contributes to 10%		
		Wavenumber 1	Wavenumber 2	Wavenumber 3
WV1	1	50	25	15
WV2	2	25	50	15
WV3	3	25	15	50
FLAT	"Flat"	30	30	30
WV12	1 and 2	35	35	20

For each signal configuration, four levels of noise are generated that account for 0%, 1%, 10%, and 20% of the total variance, respectively. The configuration for which no noise (0%) is added is chosen as a baseline (best-case scenario) and where noise contributes to 20% of the total variance represents extreme cases for which the original data would be very noisy. Cases where the noise accounts for 1% and 10% of the total variance roughly represent the noise level generally contained in the radar wind analyses (especially the horizontal wind) that motivated the present study. For $\xi > 0$, the variance explained by noise offsets the variance explained by wavenumbers 1–3, but they always amount to the same relative contribution (see Table 1 for an example where noise contribute to 10% of the total variance).

For each signal configuration and noise level, 30 signals are generated by randomly varying A_i, Φ, and ξ as explained above. Thus, a total of 600 signals are generated. Figure 2 demonstrates one example of signal generation, for configuration WV1 and 10% noise variance, where each wavenumber component and noise are generated individually (Fig. 2a) and then combined into a full signal (Fig. 2b). Figure 3 shows an example of amplitude spectra of signals of configuration WV1, WV2, and WV3 with wavenumbers 1, 2, and 3, respectively, dominating in each configuration and the noise contribution represented at the higher wavenumbers.

b. Gap insertion

For each signal generated, one to five nonoverlapping gaps of equal width are created by removing azimuthal data points. To measure the impact of gap size for a particular number of gaps, individual gap size is varied from 0° to a maximum *total* gap size never to exceed 180° (e.g., for one gap, gap size is increased up to 180°; for two gaps, gap size is varied up to 90°; etc.). This value of 180° was motivated by the fact that in the case of real observations, wavenumber 0 is often computed only if there is less than a 180° gap (note that in theory wavenumber 0 can be retrieved even with only one point present). When more than two gaps are inserted, the gaps have the same size so that each gap pattern is, to some extent, unique. Here, for brevity, we do not focus on situations with gaps of different sizes. We reason that those signals would be dominated by the largest gap present and therefore resemble the situation with one gap of the largest size. For each gap pattern, gap locations are determined randomly in 100 realizations to avoid any bias due to a specific location within the signal.

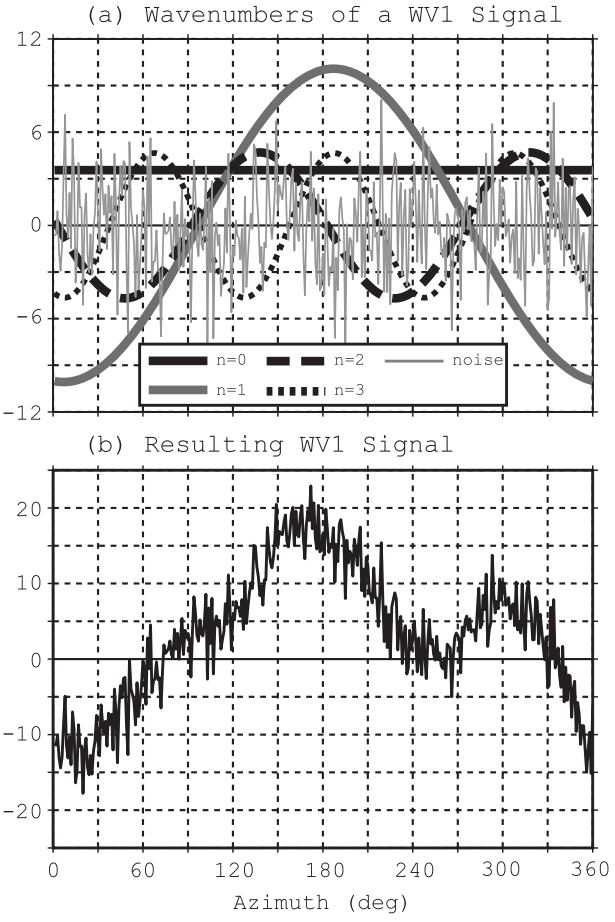

FIG. 2. (a) Wavenumber components contained in a signal of WV1 configuration and (b) the resulting signal.

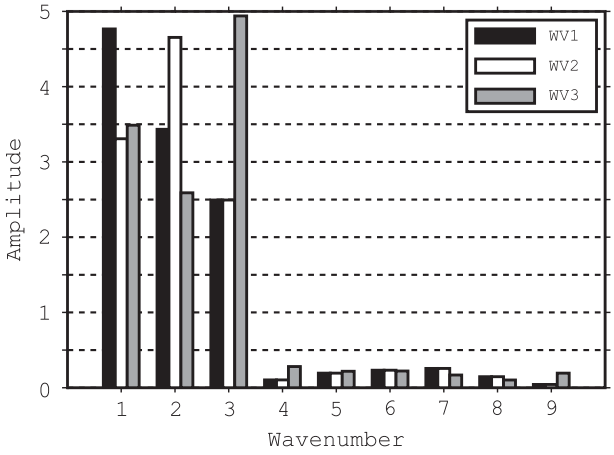

FIG. 3. Single-sided amplitude spectra resulting from configurations WV1, WV2, and WV3 with 10% of noise variance.

Figures 4a–c present an example of the procedure that generates gaps at random locations. A signal of configuration WV1 is generated, represented by the solid curves, and data are randomly removed from the signal where the locations of the gaps are depicted by the dashed lines within the curves.

c. Filling and Fourier decomposition

To perform Fourier decomposition on the gappy signals obtained as in the previous section, the gaps need to be filled first. Although many sophisticated interpolation schemes exist, a simple and computationally inexpensive filling algorithm is implemented here that generates linearly interpolated data between the end points of a given gap. Figure 4d illustrates the filling procedure applied on the signal shown in Fig. 4c.

After the gaps are filled, a fast Fourier algorithm is applied to the signals. Finally, inverse fast Fourier transforms are performed on individual wavenumber components to determine their "retrieved" amplitudes in the physical domain.

d. Evaluation metrics

Once individual wavenumbers from the filled signals are calculated (hereafter referred to as retrieved wavenumbers), they are compared to the wavenumbers of their respective original, "nongappy" signal (hereafter referred to as original wavenumbers) in terms of both amplitude and phase. The retrieval of amplitude alone would indicate how well a certain wavenumber component

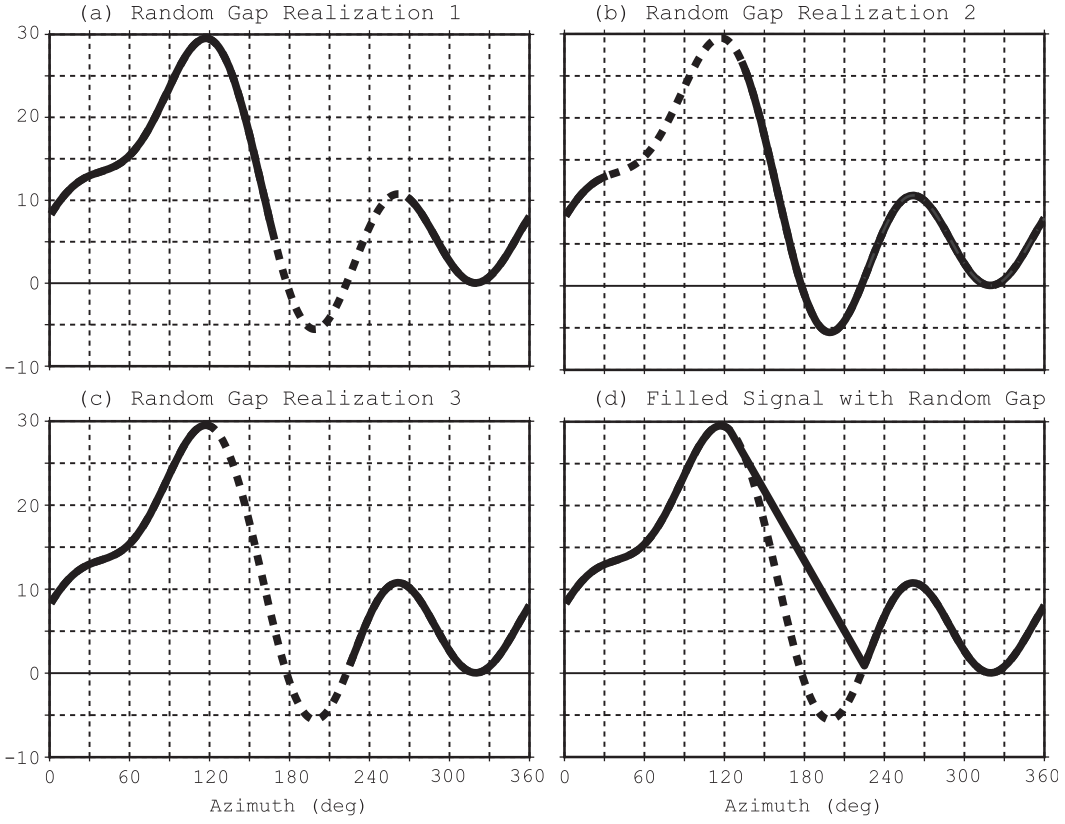

FIG. 4. Illustration of gap insertion, randomization, and filling procedures. (a),(b),(c) The same signal (solid) with various gap locations (dashed). (d) The filling procedure applied on the signal depicted in (c).

explains total variance. However, if a large error exists in the phase of the retrieved wavenumber at the same time, which means that the underlying structure is not retrieved well, one may question whether the amplitude is retrieved for the wrong reasons. Therefore, here, we focus on the accuracy of amplitude and phase simultaneously. An evaluation parameter is designed as a function of amplitude and phase as follows:

$$r_n(\Phi, A) = \frac{\mathrm{RMS}(\hat{X}_n - \tilde{X}_n)}{\mathrm{RMS}_{\max}}, \tag{3}$$

where Φ and A denote phase and amplitude, respectively; $n = 1, \ldots, 3$ is wavenumber; $\hat{X}_n$ and $\tilde{X}_n$ represent retrieved and original quantities, respectively; and RMS is short for root-mean-square defined as follows:

$$\mathrm{RMS}(\hat{X}_n - \tilde{X}_n) = \sqrt{\frac{1}{M}\sum\{[\hat{A}_n \sin(n\theta + \hat{\Phi}_n)]^2 - [\tilde{A}_n \sin(n\theta + \tilde{\Phi}_n)]^2\}}, \tag{4}$$

where M is the number of generated signals.

The parameter r therefore measures, for a given wavenumber n, the RMS of the difference between the retrieved and original wavenumber components normalized by the maximum possible value of the RMS, which occurs when the specific wavenumber components are completely out of phase ($\Phi = \pi$), resulting in the greatest difference between amplitudes. Because wavenumber 0 (azimuthal mean) does not contain any phase, r is not suitable to assess the quality of the retrieved wavenumber 0 components. For the retrieval of wavenumber 0, the retrieved value will simply be normalized directly by the azimuthal mean of the original signal and the evaluation parameter will be designated as r_0.

We choose RMS of the difference between the retrieved and original wavenumber components as the metric to measure the accuracy of retrievals as it takes into account both amplitude and phase error. Figure 5 illustrates how r can be used to evaluate the retrieved wavenumbers. If the retrieved and original wavenumbers differ only in phase (i.e., no amplitude loss), as seen in Fig. 5a, r increases with increasing phase shift, from a value of 0 when the retrieved wavenumber is identical to the original wavenumber to 1 when it is completely out of phase (Fig. 5c). If the retrieved and original wavenumbers differ only in amplitude (i.e., no phase shift), as in Fig. 5b, r varies from 0 when amplitude is fully retrieved to 0.5 when no signal for that wavenumber can be retrieved (Fig. 5d).

In more realistic cases where retrieved wavenumbers exhibit errors in both phase and amplitude, interpretation of r becomes more involved. Figure 6 represents a scenario when r is a function of both phase and amplitude error, when one value of r does not uniquely represent a specific amplitude loss or phase shift, but instead, defines a range of amplitude and phase errors. For example, an r value of 0.1 can mean that the original amplitude was fully retrieved (i.e., 0% amplitude error line) with 14° phase shift. Conversely, the same r value can also mean that the retrieved amplitude is within 80% of the original one (i.e., 20% amplitude error line) with no phase error. In other words, the best (''safest'') interpretation for $r = 0.1$ is that the retrieved amplitude is at least within 80% of the original amplitude with less than ~20° phase shift. It should be noted that there could be situations for which the amplitude of the retrieved wavenumber can slightly exceed that of the original wavenumber. However, the likelihood of such events is found to be quite minimal (not shown).

Another noteworthy result that emerges from the dual nature of r in Fig. 6 is that, beyond ~50° of phase error, it appears as though a decreasing percentage of amplitude retrieved (i.e., more amplitude error) leads to smaller r. While this result may seem self-contradictory at first, it actually only points to the fact that when retrieved and original signals are significantly out of phase, total error becomes dominated by the opposing amplitudes of the signals, so that more amplitude error results in smaller actual difference in the opposing signals, hence leading to smaller r. We therefore emphasize here that the metric r is reliable only in a small-error regime. Consequently, we will only interpret signals with r values of less than 0.1 as exhibiting acceptable retrieval quality. From the previous example, this value corresponds to a maximum of 20% loss of amplitude and ~20° phase shift error. Hereafter we will use $\hat{r} = 0.1$ to denote this threshold value.

It should be noted that the phase shift represents a phase error between the complete analyzed field and the retrieved field from the gappy data, which is different from phase errors that occur when the assumption of stationarity does not fully hold during data sampling. When analyzing wavenumbers retrieved from gappy data, one should be aware that there could be two sources of phase error: phase error inherent to the data collection method that exists even in nongappy data, and phase error due to gaps in the data.

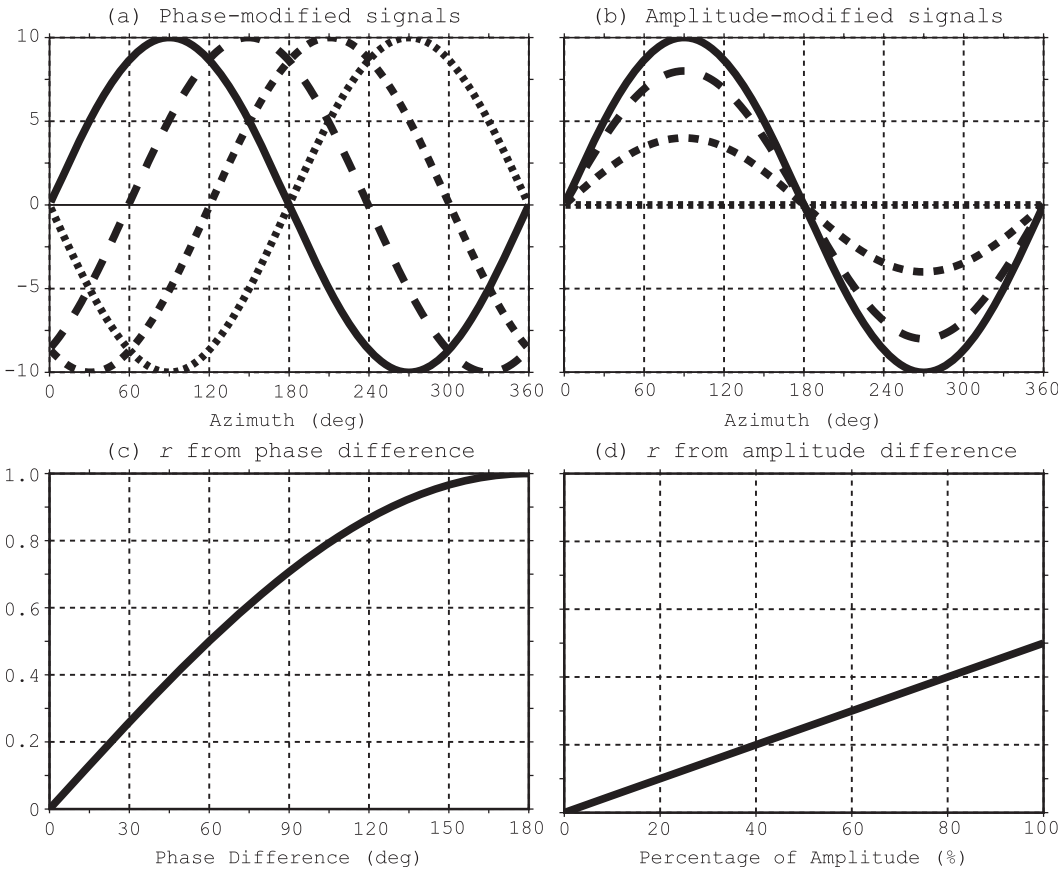

FIG. 5. (a) Example of signals (dashed) exhibiting phase shift with respect to an original signal (solid) and (c) the associated r evolution. (b) Example of signals (dashed) exhibiting amplitude loss with respect to an original signal (solid) and (d) the associated r evolution.

In the case of wavenumber 0, an 80% threshold value is chosen for an acceptable retrieval quality. Hereafter we will use $\hat{r}_0$ to denote this threshold.

3. Results

a. Determination of the maximum total gap size

The r parameter is computed for all retrieved wavenumbers and signal configurations. For a given configuration, the effect of gap size on the Fourier decomposition of particular wavenumber components is evaluated by analyzing the change of r with gap size. Our goal is, by implementing the thresholds $\hat{r}$ and $\hat{r}_0$, to deduce maximum allowable gap size for each wavenumber retrieved within each configuration.

As an example, Fig. 7 presents the variation of r with increasing total gap size and number of gaps for signal configuration WV1 with no noise (0%). The thick lines represent the mean r values while the shaded area depicts the deviation of r from its mean. For a given number of gaps, errors in the retrieved wavenumbers grow with increasing total gap size, due to greater negative impact of gap filling (interpolation) on the retrieved signal. Meanwhile, for a given total gap size, larger errors occur with fewer gaps, as this results in larger contiguous gaps and hence greater negative impact from gap filling. Therefore, from Fig. 7, the largest acceptable gap size for one gap is found by intersecting the respective error curve (thick solid line) with $r_0 = \hat{r}_0$ and $r = \hat{r}$ and for wavenumber 0 and wavenumber 1, respectively. In the rest of the analysis, we repeat this procedure for all signal configurations and wavenumbers and only report the average maximum acceptable gap size for one gap in each case. Results will be shown for cases where there is no noise added to the signal.

Figure 8a presents the resulting total maximum allowable gap size for each signal configuration and wavenumber when one gap is present in the signal. Overall, for a given wavenumber, the total allowable gap size is always the greatest when considering the configuration in which that wavenumber contributes

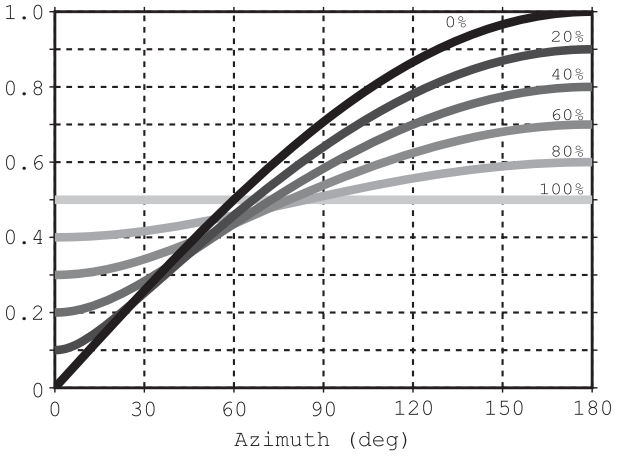

FIG. 6. Variation in r as a function of phase and amplitude error. Each line represents the evolution of r with increasing phase error for amplitude error of 0% (darkest gray shade) to 100% (lightest gray shade).

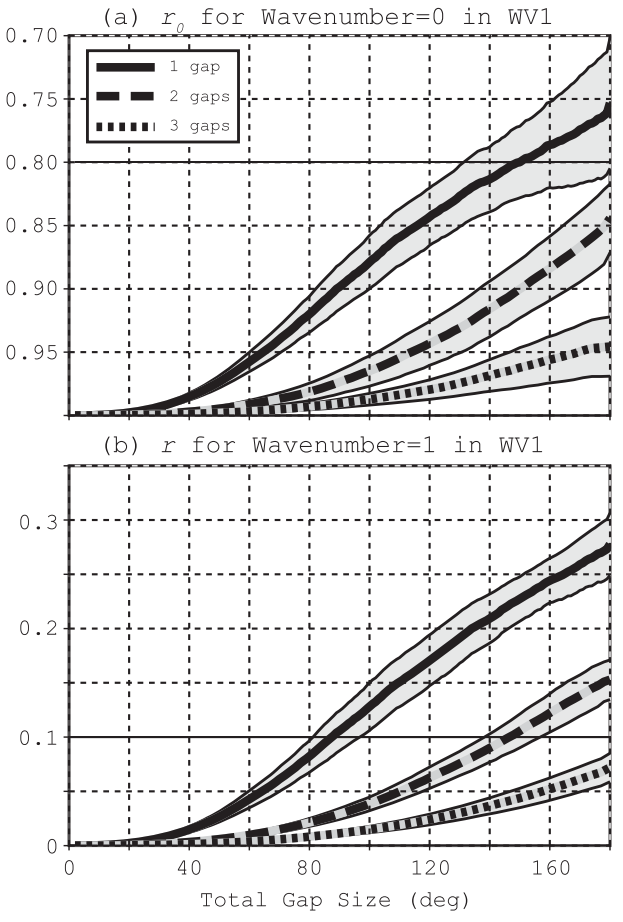

FIG. 7. Variation in r with gap size and number of gaps for WV1 configuration for (a) $n = 0$ and (b) $n = 1$. Thick lines denote mean values while the standard deviation is shown by the gray shaded envelop around the thick lines.

most to total variance. Moreover, retrieval of wavenumber 0 allows the biggest gap size compared to wavenumbers 1 and 2 in all configurations, with total maximum gap size always greater than 100°. Maximum total gap size is much smaller for wavenumbers 1 and 2 with most values under 80°. Meanwhile, the total gap size increases substantially when more than one gap is present in the signal (Fig. 8b). Figure 8b shows the maximum allowable gap size for varying gap number and all wavenumbers for configuration WV1. For wavenumber 0, when two or more gaps are present, the maximum allowable gap size reaches the maximum value of 180°. The retrieval of higher wavenumbers is also greatly impacted by the number of gaps, resulting in considerably smaller maximum allowable gap size for one gap. Maximum allowable total gap size approaches 180° when three or more gaps are present. Qualitatively similar results are obtained in other configurations.

There are situations in which a more restrictive threshold value $\hat{r}$ could be preferred. For example, if one is requiring a very accurate assessment of the wavenumber amplitude, obtaining an amplitude within 90% of the original amplitude might be desired. For this case, a new threshold value $\hat{r} = 0.05$ would be used. This new threshold value would also reduce the phase error criterion to less than 10°. The maximum gap size allowed in this scenario, for all configurations with one gap and no noise is presented in Fig. 9a and shows that the maximum gap sizes are very limited, with all values under 90°. On the other hand, if one is interested in a rather qualitative study of the wavenumber structure, the threshold value could be relaxed. A threshold value $\hat{r} = 0.15$, would allow the magnitude of the retrieved wavenumber to be within 70% of the original amplitude, with a phase shift still smaller than 20°. Figure 9b shows the resulting maximum gap size for this threshold value, for the same signal configuration as in Fig. 9a. For this threshold, the maximum gap size allowed to retrieve wavenumber 0 reaches the maximum value of 180° for all configurations. For wavenumbers 1 and 2 the maximum gap sizes allowed increase but the increase seems to be dependent on the importance of the wavenumber in the signal. For instance, when wavenumber 2 contributes most to the signal (i.e., WV2), the increase is greater than 20° whereas when it contributes the least in the signal (WV3), the increase is only by a few degrees.

The impact of the noise is also evaluated. The addition of noise reduces the total variance contributed by the wavenumbers, which would result in a more challenging retrieval. Figure 10 illustrates the impact of noise on the maximum allowable gap size for wavenumber 1 retrieval, when one (Fig. 10a) or three (Fig. 10b) gaps are

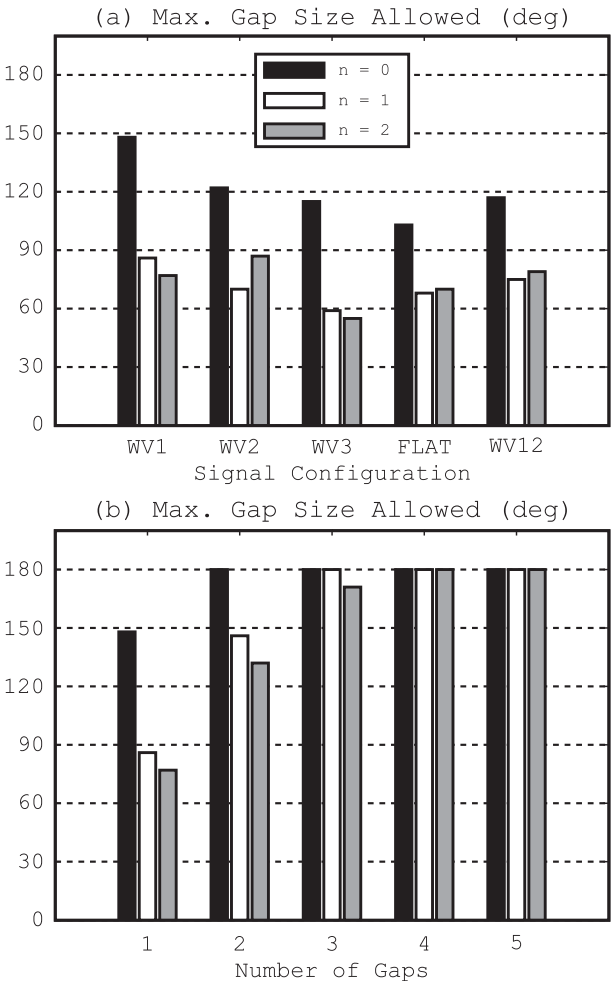

FIG. 8. Maximum gap size allowed for wavenumbers 0–2 for (a) all five signal configurations when one gap is present in the signal and (b) various numbers of gaps for WV1 configuration.

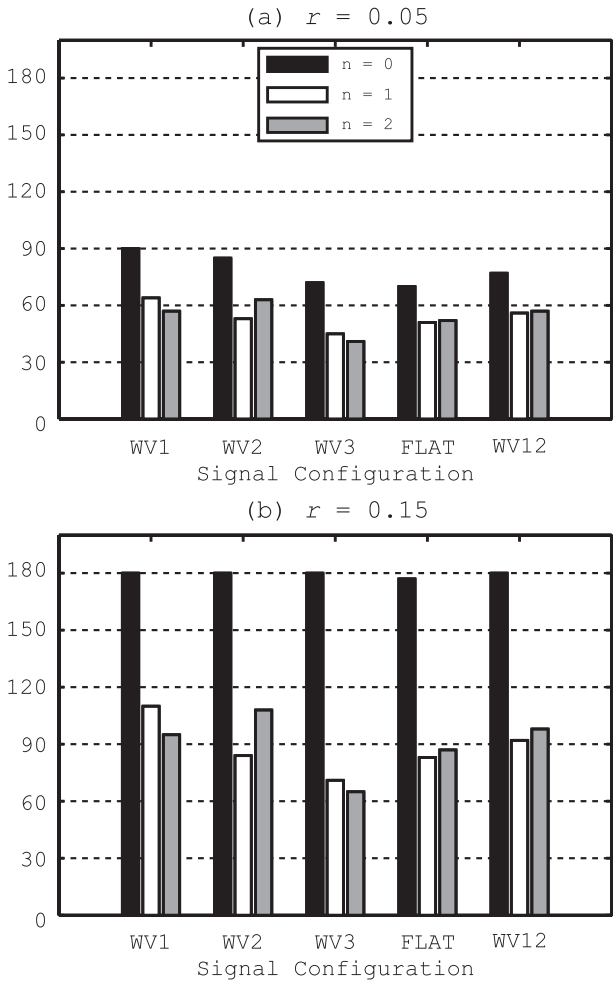

FIG. 9. Maximum gap size allowed for wavenumbers 0–2 for all five signal configurations when one gap is present in the signal for (a) $\hat{r} = 0.05$ and (b) $\hat{r} = 0.15$.

present in the signal. Smaller noise levels provide slightly better results as smaller noise decreases errors in the retrieval and hence increases the maximum allowable gap size. Meanwhile, the number of gaps in the signal also impacts the results. More gaps present in the signal generally result in a greater drop in allowable gap size.

The results described above are obtained with a mean (wavenumber 0) signal value equal to the amplitude of the most energetic wavenumber(s) of each considered signal configuration. This allows for a relatively nonchallenging wavenumber 0 retrieval. However, wavenumber 0 retrieval becomes more challenging when the assumed mean signal value is smaller than the amplitude of the most energetic wavenumber(s). To assess the impact of the mean signal value on the retrieval and therefore on total allowable gap size, the one-gap experiment above is repeated where the mean signal value is varied from 20%–100% of the amplitude of the wavenumber that contributes the most to total variance. Results are summarized in Fig. 11 and clearly show that the accuracy of retrieval of wavenumber 0 is highly dependent on the relative mean signal strength. For a WV1 configuration, for example, the maximum allowable gap size is restricted to 40° when the mean signal is only 20% of the wavenumber 1 amplitude. Such configuration can be found in the radial wind field of landfalling tropical cyclones, where wavenumber 1 amplitude can significantly exceed the mean radial wind (Liou et al. 2006). On the other hand, the maximum allowable gap size is 145° when the mean signal and wavenumber 1 amplitude are comparable. This type of configuration has been documented in real observations (Roux and Marks 1996; Marks et al. 1992). These findings are critical to perform the widely used radius–height azimuthal means of gappy

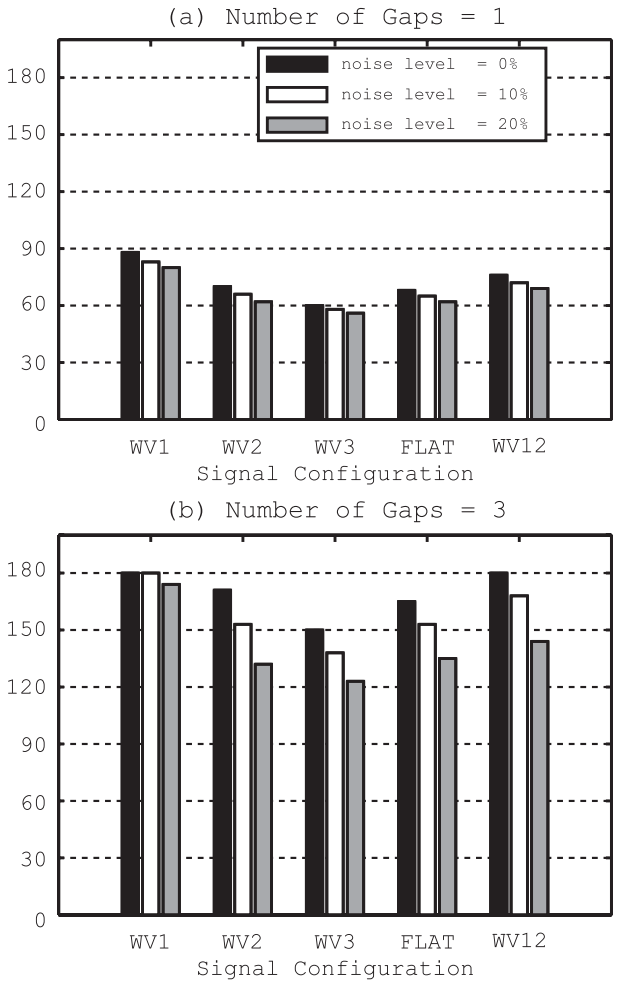

FIG. 10. Maximum gap size allowed for wavenumber 1, all configurations and noise contributing to 0%, 10%, and 20% of total variance when (a) one gap and (b) three gaps are present in the signal.

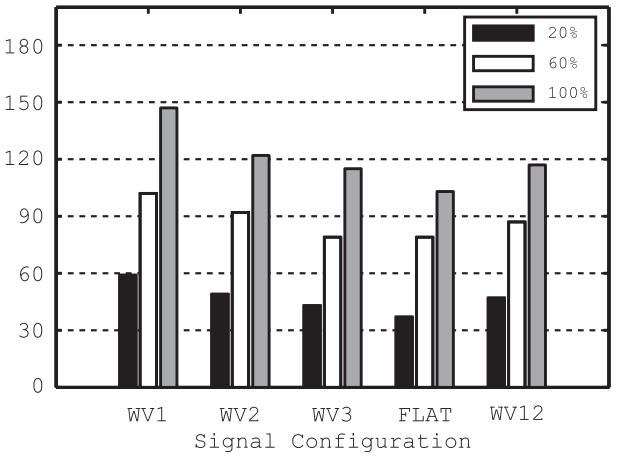

FIG. 11. Maximum gap size allowed for wavenumber 0 when its amplitude is 20%–100% of the amplitude of the most energetic wavenumber(s). Experiment performed for all configurations when one gap is present.

data and should be considered when computing these means.

b. An example from real observations

The present study stems from the need to better understand the kinematic structure of TCs by analyzing the various wavenumbers contained in fields such as tangential wind and vorticity. In the previous sections, we focused on synthetic data where gaps were inserted to simulate missing data often encountered in real observations and more specifically in Doppler data analyses. An example from a real case is now presented to illustrate how the methodology can be applied to real data. Figure 12a shows a radial wind analysis from Hurricane Guillermo (1997). The data were acquired with the tail Doppler radar of a National Oceanic and Atmospheric Administration (NOAA) WP-3D (P-3) aircraft. The wind field exhibits a strong wavenumber 1 component at all radii, but higher wavenumbers are also clearly visible as seen at ~20 km from the center. The wind field displays large azimuthal gaps (>130°) of missing data beyond 60 km from the storm center, while between 20 and 60 km there are in general two gaps of total size smaller than 130°. Inside the 20-km radius, there are places with one gap of small size. Based on the results presented in section 3a (Fig. 7b), the gap size criteria are met up to 60 km and wavenumber 1 retrieval for this field may therefore be performed. Figure 12b presents the resulting wavenumber 1 field computed from the radial wind field after the gaps were filled in the same manner as explained previously, exhibiting a rather realistic distribution compared to the original field. Wavenumbers 0 and 2 can be retrieved following a similar procedure and the guidance provided for WV1 configuration.

4. Conclusions and recommendations

In this study, a Monte Carlo–type experiment is conducted to assess the maximum gap size to be allowed when performing Fourier analysis on ''gappy'' azimuthally distributed data. Numerous signals of various wavenumber configurations and noise levels are generated with gaps of varying size. A simple linear interpolation scheme is then applied and Fourier decomposition is performed. The wavenumber decomposition is evaluated in a way that requires retrieval of at least 80% of the original amplitude with less than 20° phase shift. The results indicate that, when two or more gaps are present in the signal, the maximum gap size allowed is greater than originally suggested in the literature (Lee et al. 2000).

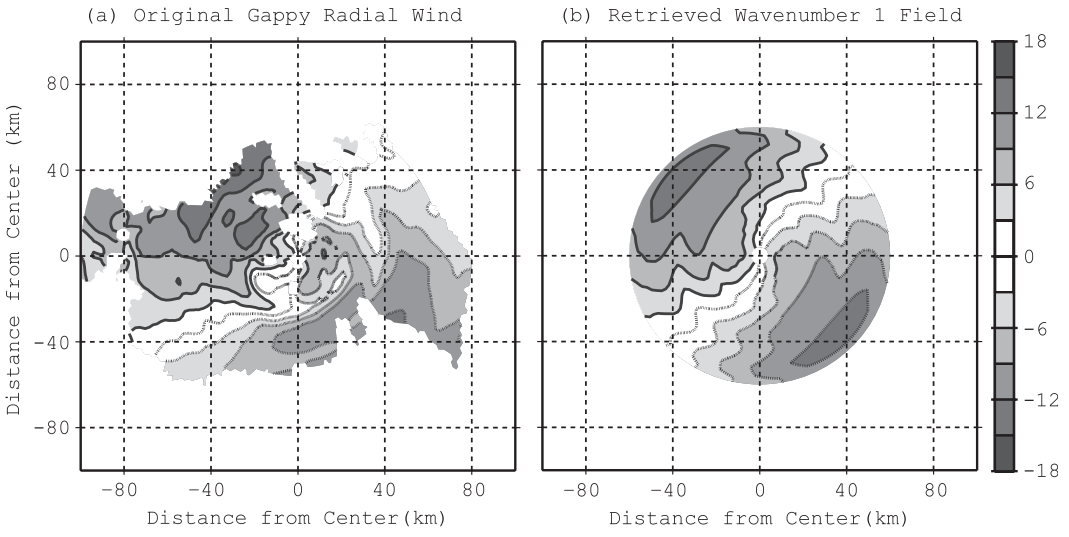

FIG. 12. Real observation case. (a) The radial wind from Hurricane Guillermo (1997) at 2-km height and (b) the resulting wavenumber 1 field. Solid lines and dashed lines delineate positive and negative values, respectively.

Increasing noise negatively impacts the maximum gap size allowed. It is also found that the impact of noise is amplified when there are more gaps in the signal. However, noise does not appear to influence the relative distribution of the maximum allowable gap size among various wavenumber configurations.

We also found that wavenumber components are best retrieved when they contribute most to total variance. Wavenumber 0 is retrieved with most accuracy when its amplitude (i.e., mean signal value) is at least equal to the amplitude of the wavenumber that contributes the most to the total variance. It should be noted that, since errors in both amplitude and phase are quite restricted, aliasing that can arise with large gaps in the signal is not expected to impact results negatively here.

The results described here can serve as a reference when dealing with azimuthally distributed gappy data and the guidance provided here can be extended to other atmospheric phenomena and datasets. Indeed, the present methodology can be applied to phenomena for which data are azimuthally distributed such as tornados or other types of vortices. Gaps in tornado radar datasets due to sidelobes effect and ground clutter due to trees and buildings can seriously impede wavenumber analysis (Bluestein et al. 2003); the present method can be applied in a similar manner to deal with issues posed by missing data. Although the case described in Bluestein et al. (2003) was wavenumber 2 dominant and the results provided here could be applicable to such a case, it is not necessarily obvious whether the signal configurations used in the present study would be generally applicable to observed tornado wavenumber configurations, as higher wavenumbers might contribute more to the total variance. The method could even be extended to point measurement data such as tightly clustered mobile mesonet instruments. To apply the present results to this type of dataset, however, it would be crucial that the density of the data allow for more than just the resolution of the signal wavenumbers, which would require an extensive amount of instruments.

For the particular problem of Fourier decomposition of gappy Doppler radar analyses that motivated the present study, results using two gaps will be most important, as it is the most common gap pattern found in this type of data. Also, the results presented here can be most useful when the wavenumber to be studied contributes most to total variance, which is generally the case. Finally, although one does not usually know the exact wavenumber configuration of an observed signal or the importance of a particular wavenumber, prior information (from earlier time period or other altitude), knowledge of physical processes that contribute to the signal, or availability of alternate data sources all can lead to a general expectation of a particular signal configuration. Especially when such prior assessment of signal configuration is available, we believe that the present study can provide valuable guidance for gap size beyond which Fourier decomposition is not advisable.

Acknowledgments. The authors acknowledge funding from the NOAA Hurricane Forecast Improvement Project that supported this work. This research was carried out (in part) under the auspices of CIMAS,

a joint institute of the University of Miami and NOAA, Cooperative Agreement NA67RJ0149. The authors thank Dr. Paul Reasor, Dr. John Gamache, and the anonymous reviewers for their insightful input.

REFERENCES

Aberson, S. D., M. Black, M. T. Montgomery, and M. Bell, 2006: Hurricane Isabel (2003): New insights into the physics of intense storms. Part II: Extreme localized wind. *Bull. Amer. Meteor. Soc.,* **87,** 1349–1354.

Bluestein, H. B., W.-C. Lee, M. Bell, C. C. Weiss, and A. L. Pazmany, 2003: Mobile Doppler radar observations of a tornado in a supercell near Bassett, Nebraska, on 5 June 1999. Part II: Tornado-vortex structure. *Mon. Wea. Rev.,* **131,** 2968–2984.

Gamache, J. F., 1997: Evaluation of a fully three-dimensional variational Doppler analysis technique. Preprints, *28th Conf. on Radar Meteorology,* Austin, TX, Amer. Meteor. Soc., 422–423.

Gao, J., M. Xue, A. Shapiro, and K. K. Droegemeier, 1999: A variational method for the analysis of three-dimensional wind fields from two Doppler radars. *Mon. Wea. Rev.,* **127,** 2128–2142.

Lee, W.-C., B. J.-D. Jou, P.-L. Chang, and F. D. Marks, 2000: Tropical cyclone kinematic structure retrieved from single-Doppler radar observations. Part III: Evolution and structures of Typhoon Alex (1987). *Mon. Wea. Rev.,* **128,** 3982–4001.

Liou, Y.-C., T.-C. Chen Wang, W.-C. Lee, and Y.-J. Chang, 2006: The retrieval of asymmetric tropical cyclone structures using Doppler radar simulations and observations with the Extended GBVTD technique. *Mon. Wea. Rev.,* **134,** 1140–1160.

Marks, F. D., Jr., R. A. Houze Jr., and J. F. Gamache, 1992: Dual-aircraft investigation of the inner core of Hurricane Norbert. Part I: Kinematic structure. *J. Atmos. Sci.,* **49,** 919–942.

Montgomery, M. T., and R. J. Kallenbach, 1997: A theory for vortex Rossby waves and its application to spiral bands and intensity changes in hurricanes. *Quart. J. Roy. Meteor. Soc.,* **123,** 435–465.

——, M. M. Bell, S. D. Aberson, and M. L. Black, 2006: Hurricane Isabel (2003): New insights into the physics of intense storms. Part I: Mean vortex structure and maximum intensity estimates. *Bull. Amer. Meteor. Soc.,* **87,** 1335–1347.

Nolan, D. S., D. P. Stern, and J. A. Zhang, 2009: Evaluation of planetary boundary layer parameterizations in tropical cyclones by comparison of in situ data and high-resolution simulations of Hurricane Isabel (2003). Part II: Inner core boundary layer and eyewall structure. *Mon. Wea. Rev.,* **137,** 3675–3698.

Reasor, P. D., M. T. Montgomery, F. D. Marks Jr., and J. F. Gamache, 2000: Low-wavenumber structure and evolution of the hurricane inner core observed by airborne dual-Doppler radar. *Mon. Wea. Rev.,* **128,** 1653–1680.

——, M. Eastin, and J. F. Gamache, 2009: Rapidly intensifying Hurricane Guillermo (1997). Part I: Low-wavenumber structure and evolution. *Mon. Wea. Rev.,* **137,** 603–631.

Roux, F., and F. D. Marks, 1996: Extended Velocity Track Display (EVTD): An improved processing method for Doppler radar observations of tropical cyclones. *J. Atmos. Oceanic Technol.,* **13,** 875–899.

Schubert, W. H., M. T. Montgomery, R. K. Taft, T. A. Guinn, S. R. Fulton, J. P. Kossin, and J. P. Edwards, 1999: Polygonal eyewalls, asymmetric eye contraction, and potential vorticity mixing in hurricanes. *J. Atmos. Sci.,* **56,** 1197–1223.